Atmospheric Chemistry and Physics Discussions

Atmospheric column-averaged mole fractions of carbon dioxide at 53 aircraft measurement sites

Y. Miyamoto[1,*], M. Inoue[1], I. Morino[1], O. Uchino[1], T. Yokota[1], T. Machida[1], Y. Sawa[2], H. Matsueda[2], C. Sweeney[3], P. P. Tans[3], A. E. Andrews[3], and P. K. Patra[4]

[1]National Institute for Environmental Studies (NIES), Tsukuba, Japan
[2]Meteorological Research Institute (MRI), Tsukuba, Japan
[3]National Oceanic and Atmospheric Administration (NOAA), Boulder, CO, USA
[4]Japan Agency for Marine-Earth Science and Technology (JAMSTEC), Yokohama, Japan
[*]now at: Graduate School of Nature Science and Technology, Okayama University, Okayama, Japan

Correspondence to: I. Morino (morino@nies.go.jp)

ACPD

12, 28493–28523, 2012

Atmospheric XCO$_2$ from aircraft measurements

Y. Miyamoto et al.

Title Page

Abstract	Introduction
Conclusions	References
Tables	Figures

|◄ | ►|
◄ | ►

Back | Close

Full Screen / Esc

Printer-friendly Version

Interactive Discussion

Abstract

Atmospheric column-averaged mole fractions of carbon dioxide (XCO$_2$) at 53 locations around the world were derived from aircraft measurements covering the altitude range of about 1–10 km. We used CO$_2$ vertical profile measurements from three major carbon
5 cycle programs, a global climatological data set of air number density profiles and tropopause height for calculating XCO$_2$ for the period of 2007–2009. Vertical profiles of the CO$_2$ mixing ratio are complemented by tall tower data up to 400 m from the earth's surface and by simulated profiles in the stratosphere from a chemistry-transport model. The amplitude of the seasonal cycle of calculated XCO$_2$ values shows clear latitudinal
10 dependence, and the amplitude decreases from about 10 ppm at high latitudes in the Northern Hemisphere to at most 2 ppm in the tropics and the Southern Hemisphere. The uncertainties of XCO$_2$ were estimated from assumptions about CO$_2$ profiles for each flight. Typically, uncertainties were less than 1 ppm; thus, this data set is within the level of uncertainty needed for primary validation of XCO$_2$ measurements by the
15 Greenhouse gases Observing SATellite (GOSAT) and by future satellite missions for monitoring greenhouse gases.

1 Introduction

Atmospheric abundance of CO$_2$ has drawn great interest in the recent decade because CO$_2$ is the most important anthropogenically produced greenhouse gas (WMO, 2006).
20 The Greenhouse gases Observing SATellite (GOSAT), launched on 23 January 2009, is equipped with a Fourier transform spectrometer (FTS) to observe the atmospheric column-averaged mole fraction of CO$_2$ (XCO$_2$) at more uniform geographical coverage than the in situ measurement network (WDCGG, 2012). GOSAT overpasses the region from 80° S to 80° N in longitudinal bands every 3 days. From 4 April 2009 to 31 July
25 2010, observational points were ∼ 158 km apart cross-track and ∼ 152 km apart along-track at the equator with the 5 point cross-track scan mode, and since 1 August 2010,

observational points are ~ 263 km apart cross-track and ~ 283 km apart along-track at the equator with the 3 point cross-track scan mode (Yokota et al., 2009; Kuze et al., 2009; Yoshida et al., 2011). In contrast, the in situ measurement network comprised of fewer than 216 sites (WDCGG, accessed 10 October 2012). XCO_2 measurements by remote sensing equipments will provide another perspective for studying the carbon cycle processes by better constraining the surface fluxes through inverse modeling. Modeling studies have shown that uncertainty of the source/sink inversion results is linked to the error of the satellite CO_2 measurements (e.g. Rayner et al., 2002; Patra et al., 2003). Miller et al. (2007) showed that precisions of 1–2 ppm in XCO_2 satellite measurements are needed to improve our knowledge of carbon cycle phenomena. Therefore, it is important to evaluate the quality of data obtained from satellites by comparing them with more accurate, though sparse, in situ observations.

Because of their high accuracy, aircraft profile measurements are used for comparison with satellite data, but these measurements are limited in frequency and spatial density. Recently, the CONTRAIL (Comprehensive Observation Network for TRace gases by AIrLiner) project, by using commercial airplanes, has succeeded in measuring frequent and vertically dense data over a number of airports (Machida et al., 2008). CO_2 mixing ratios recorded during takeoff and landing can be used to calculate XCO_2 above airports.

Another XCO_2 data set useful for validating satellite data is from the Total Carbon Column Observing Network (TCCON, Wunch et al., 2010, 2011a,b; Morino et al., 2011; Schneising et al., 2012), a ground-based FTS network. The measurement uncertainty of the FTS system, which has been certified by aircraft measurements, is similar to that of them, and the FTS network covers a wider area, but the number of aircraft measurements sites are greater than that of the TCCON sites.

Araki et al. (2010) reported XCO_2 values calculated over Tsukuba, Japan, from CONTRAIL data obtained at Narita Airport and ancillary data sets. They also estimated the uncertainty derived from the assumptions made about the air density profile, the tropopause height, and the CO_2 profile near the surface.

In this study, we report the results of XCO_2 calculations carried out with data provided by CONTRAIL, measurements made by the US National Oceanic and Atmospheric Administration (NOAA) and the National Institute for Environmental Studies (NIES), Japan at 53 sites between 2007 and 2009. The method used in this study is similar to that of Araki et al. (2010), but the treatment of the stratospheric vertical profile has been improved. Section 2 briefly describes the measurements by CONTRAIL, NOAA, and NIES. Section 3 presents details of the calculation of XCO_2 and estimation of its uncertainty. In Sect. 4, the results of the calculation of XCO_2 temporal behavior are presented and their uncertainties are discussed.

2   Observations

Aircraft measurements obtained by CONTRAIL, NOAA, and NIES between 2007 and 2009 were used in this study. Details of each project have been reported elsewhere (Machida et al., 2008; Machida et al., 2001; Tans et al., 1996; ESRL/GMD CCGG Aircraft Program, 2011) and are only described briefly here. The locations of the CONTRAIL, NOAA, and NIES observations are shown in Fig. 1, and they are listed along with their three-letter site codes in Table 1.

The CONTRAIL project takes advantage of the numerous flights made by commercial airlines worldwide to acquire frequent measurements of CO_2 at a relatively large number of sites. Automatic air sampling equipment for discrete sampling and continuous CO_2 measuring equipment (CME) for in situ observations are installed onboard aircraft operated by Japan Airlines. XCO_2 is calculated from the data obtained by CME upon departure from and arrival at 28 different airports. These profiles differ from those obtained by the NOAA and NIES aircraft because the commercial aircraft move horizontally over a few hundred kilometers during their takeoff and landing. The data are typically collected at altitudes between a few kilometers and 10 km (Machida et al., 2008). Measurements are not carried out at regular time intervals at all locations. For example, there were 10 flights in May 2007 and only 2 flights in April 2007 at Schiphol

Airport (AMS, Amsterdam, the Netherlands). The CME observations are calibrated on-board the airplane with standard gases based on NIES 09 CO_2 scale, which is closed to World Meteorological Organization (WMO) standards (Machida et al., 2011) at 10 min intervals during ascending and descending and at 40 min intervals during cruising. The uncertainty of the CME observations is estimated to be about 0.2 ppm (Machida et al., 2008).

The NOAA measurements are from an aircraft observation network of 21 sites operated by the Global Monitoring Division of the Earth System Research Laboratory (GMD/ESRL). Flask sampling observations are performed several times a month, and the reported uncertainty is ~ 0.15 ppm. The typical altitude range is from a few hundred meters to 5–8 km above ground level (ESRL/GMD CCGG Aircraft Program, 2011; http://www.esrl.noaa.gov/gmd/ccgg/aircraft/index.html).

The measurements by NIES are made by flask sampling at three sites in Russia and one site in Japan. Sampling frequency is once or twice a month. Typical observing altitudes are 0.5–7 km. The uncertainty is estimated to be 0.2 ppm, which takes into account the scale difference between standard gases (Machida et al., 2001).

3 Method

The calculation method used in this study is basically equivalent to that used by Araki et al. (2010) in their analysis, with the following modifications, mainly to make the method applicable to places anywhere in the world.

The vertical profiles of the CO_2 mixing ratios in dry air are calculated from aircraft measurements made over a limited altitudinal range. Therefore, to calculate XCO_2, additional information is needed: (1) supplemental vertical profiles of CO_2 in the altitude range where observation data are not available, and (2) vertical profiles of the dry air number density above the sites. In this study, similar to Araki et al. (2010), these two types of profiles (CO_2 mixing ratio and the dry air number density) were prepared from ground level to 85 km above the ground.

Title Page

Abstract	Introduction
Conclusions	References
Tables	Figures

◄◄ ►►

◄ ►

Back Close

Full Screen / Esc

Printer-friendly Version

Interactive Discussion

To construct stratospheric profiles, Araki et al. (2010) used an empirical model of CO$_2$ profiles at mid-latitudes in the Northern Hemisphere. In this model, the concentration is assumed to be constant above 20 km and values between the tropopause and 20 km are obtained by linear interpolation. In this study, profiles derived from the modeled "age of air" were used to calculate XCO$_2$ at various latitudes. The age of air was obtained from simulations by the atmospheric general circulation model-based chemistry-transport model (ACTM) of the NIES/Center for Climate System Research/Frontier Research Center for Global Change (Patra et al., 2009). The modeled age of air was compared with ages estimated by using several vertical profiles of sulfur hexafluoride (SF$_6$) in the upper troposphere and stratosphere in the latitude range of 17–70° N, based on measurements made by balloon-borne instruments (Harnisch et al., 1996; Patra et al., 1997), to obtain correction factors at each profile location. The correction factors at each profile location were then interpolated and applied to all model grid cells between the equator and the North Pole. The mirror image was used for the Southern Hemisphere under the assumption that the age of air in the stratosphere is determined by vertical mixing at the equator (e.g. Andrews et al., 2001; Austin and Li, 2006). The ages were converted to CO$_2$ mixing ratios by assuming that the tropospheric concentration (corresponding to 0-yr-old mixing ratio) in 2006 was 381.2 ppm and that the annual increasing trend was 1.9 ppm yr^{-1} at every site (WMO, 2006). This study estimated the mean age to be about 5–6 yr in the mid-latitude stratosphere (24–50 km). This result is consistent with the findings of other recent studies on the age of stratospheric air (e.g. Ishidoya et al., 2008; Engel et al., 2009). Zhu et al. (2000) showed that the mean age of air is about 6.5 yr at 80 km by using a globally balanced two-dimensional middle atmosphere model. The amount of CO$_2$ above 50 km is so small that assumptions about the profile above 50 km do not affect the results within the uncertainties. Therefore, the modeled profile was used up to 50 km, and above 50 km the mixing ratio was assumed to be constant at the 50-km value. The CO$_2$ profiles derived from the age of air have been compared with measurements of CO$_2$ made by balloon-borne instruments over Japan from 1987 to 2007 at Sanriku (39.1° N, 141.8° E) (Nakazawa et al.,

1995). These data show an increasing trend of 1.52 ppm yr^{-1}, so all data were normalized to 1 January 2007 using this value. The trend obtained at Sanriku differs from the world-average trend of 1.9 ppm yr^{-1} in 2000's because it was determined by data collected over a different period (1996–2005). The normalized data were averaged within each altitude range: 15–20, 20–25, 25–30, and above 30 km. The uncorrected model clearly underestimated the age of air at most heights, particularly in the lower stratosphere (Fig. 2). When the SF$_6$-corrected model ages were used, the age-based CO$_2$ reconstruction successfully reproduced the observed rate of decrease for CO$_2$ with increasing altitude in the stratosphere within a deviation of about 1.3 ppm (root mean square). In this study, monthly averaged ACTM profiles were used after interpolating to the site location.

When the top measurement height was below the tropopause, the concentration measured at the highest altitude was assumed to be maintained up to the tropopause. The local tropopause height was obtained from the US National Centers for Environmental Prediction (NCEP) Global Forecast System (GFS), a global spectral numerical model based on primitive dynamical equations that includes a suite of parameterizations for atmospheric physics (Sela, 1980; Kalnay et al., 1990). The model is under constant development and evaluation (e.g. Yang et al., 2006).

To extrapolate profiles to the surface, tower data obtained at the Meteorological Research Institute (Tsukuba, 36.1° N, 140.1° E), the LEF, WBI, and WGC towers were used for aircraft measurements obtained over Narita airport (Japan, NRT), Park Falls (Wisconsin, LEF), West Branch (Iowa, WBI) and Walnut Grove (California, WGC), respectively (Inoue and Matsueda, 1996, Andrews et al., 2011). Tower data for NOAA sites were acquired from the NOAA web site (GMD Data Archive).

The concentration at the lowermost observation above the planetary boundary layer (PBL) was assumed to hold from that point to the top of the PBL. When there were observed data within the PBL, the concentration at the highest observation height within the PBL was extended to the PBL top, and that at the lowest observation height was extended to ground level. When there were no observation data within the PBL, the

concentration of the lowermost observation above the PBL was assumed to hold to ground level. Local PBL heights for each site were obtained from NCEP GFS.

Figure 3 shows a schematic example of a profile constructed with these assumptions. Discontinuities between the observed profiles and ACTM stratospheric profiles were at most a few ppm (mean $\sim$ 1 ppm, standard deviation $\sim$ 1 ppm). No correction was applied to resolve this discontinuity, but it is considered to be a source of uncertainty in the assumed profile, as discussed in Sect. 4.

The profiles of dry air number density were calculated by using the data sets of monthly mean climatological temperature and pressure of the Committee on Space Research (COSPAR) International Reference Atmosphere (CIRA)-86 (e.g. Fleming et al., 1988, 1990), which are given at 5° latitude intervals between 80° N and 80° S for altitudes of 0 to 120 km. Values at each observation site were obtained by linear interpolation of CIRA-86 data between two 5° grid points. Monthly mean values were adopted without interpolation in time.

XCO$_2$ was calculated by numerical integration of CO$_2$ dry mole fractions weighted by the dry air density within 100-m layers from the ground up to 85 km. It was assumed that the atmosphere was well mixed within each layer. Column abundance above 85 km was roughly estimated to be less than 0.01 %, which is small enough to be neglected in this study. If the CO$_2$ mixing ratio (mole CO$_2$/mole air) and dry air number density in the ith layer are $n(i)$ and $N(i)$, respectively, XCO$_2$ can be represented as

$$XCO_2 = \sum_{surface}^{85\,km} n(i) \times N(i)/N, \qquad (1)$$

where N is the total column abundance of dry air; $N(i)$ is calculated by logarithmic interpolation of the vertical profile of CIRA-86 data with a vertical resolution of 2 km; and $n(i)$ is calculated by linear interpolation between two neighboring observed or constructed data points. Araki et al. (2010) used only clear sky data for their analysis, whereas no screening by the weather conditions was done in this study.

Full Screen / Esc

Printer-friendly Version

Interactive Discussion

The uncertainty of the XCO$_2$ calculation caused by the profile assumptions was estimated for each flight. In this study, the focus is on the upper limit of the uncertainty, because that value is most important for the validation of satellite observations. Because XCO$_2$ is the weighted mean of CO$_2$ concentrations calculated by the dry air abundance in each layer, its uncertainty was determined by the assumed uncertainties of the partial XCO$_2$ values and their weights. In this study, the uncertainty was defined as the standard deviation. We did not take into account the uncertainty of the dry air number density $N(i)$ (i.e. no variance) in this study because the XCO$_2$ values calculated by using the CIRA-86 number densities agreed with rawinsonde values obtained over Tsukuba within 0.1 ppm (Araki et al., 2010). The profiles were divided into four domains, within each of which the uncertainty of the data was treated as uniform: domain I, inside the PBL; domain II, region above the PBL with observed data; domain III, troposphere above the PBL without observed data; and domain IV, stratosphere without observed data. The uncertainty of total XCO$_2$ is represented as follows:

$$\text{Uncertainty} = \frac{\sqrt{\sum_j N(j)^2 \times \sigma(j)^2}}{N} \quad (j = \text{I, II, III, IV}), \tag{2}$$

where $\sigma(j)$ and $N(j)$ are the assumed uncertainty of partial XCO$_2$ and the partial dry air number density in the j-th domain, respectively, and N is the total sum of $N(j)$. Based on data comparisons, $\sigma(\text{I})$ was assumed to be 15 ppm for flights with no data in the PBL or 2.89 ppm (corresponding to a uniform distribution within ±5 ppm) for flights with data in the PBL. $\sigma(\text{II})$ was assumed to be 0.4 ppm, and $\sigma(\text{III})$ and $\sigma(\text{IV})$ were assumed to be 1.73 ppm (corresponding to a uniform distribution within ±3 ppm) (Table 2). The total uncertainty was determined from the height of the tropopause and the PBL, the uppermost and lowermost observation altitudes, the partial dry air abundances $N(j)$, and the uncertainties of partial XCO$_2$ $\sigma(j)$. The values of $\sigma(j)$ are critical for the estimation of total uncertainty, and their validity is discussed in Sect. 4.

4   Results and discussion

Figure 4 shows the calculated XCO_2 values and their uncertainties derived from the profile assumptions at the 53 sites between 2007 and 2009. As a visual guide, the following function was fitted to the XCO_2 data:

$$XCO_2(t) = a_1 + a_2 \times t + a_3 \times \cos\left(2\pi\frac{t-a_4}{365.25}\right) + a_5 \times \cos\left(4\pi\frac{t-a_6}{365.25}\right) \qquad (3)$$

where a_1 is the intercept at the zero time point (1 January 2007) without sinusoidal variations, a_2 represents the yearly trend of XCO_2, a_3 and a_5 are the amplitudes of sinusoidal variations with a period of one year and a half year, respectively, and a_4 and a_6 are the phases of each sinusoidal variation. Annual sinusoidal variations and their latitudinal dependence are clearly seen. The amplitude of the seasonal cycle decreases from about 10 ppm at high latitudes in the Northern Hemisphere to 2 ppm or less in the tropics and the Southern Hemisphere. Compared with XCO_2 at NRT in 2007, calculated by Araki et al. (2010), the temporal behavior of XCO_2 is typically the same within our uncertainties.

The uncertainty estimation can be validated by comparing the partial XCO_2 value calculated from the observed profile with the fitted profile for each domain. For domain I (PBL), the data sets containing observed data in the PBL were chosen and the CO_2 concentrations at 5 km and 200 m were compared with the partial XCO_2 in the PBL. The concentration at 5 km corresponds to the partial XCO_2 assumed when a profile has no observed data in the PBL. The concentration at 200 m corresponds to the partial XCO_2 assumed when a profile has only one observed datum in the PBL. For this analysis, sites that had sufficient observations in the PBL to evaluate the "true" partial XCO_2 in the PBL were chosen. Therefore, sites with tower data were used for this analysis. The root mean square (RMS) of the deviation of the assumed partial XCO_2 from the observed partial XCO_2 was calculated. These comparisons show that the RMS in domain I was less than 3 ppm for flights with PBL data observations, and it was

at most 15 ppm for flights without PBL data. These values agree with our assumptions about partial uncertainties.

For domain II (observation region above the PBL), the reported standard deviation of the measurements was typically 0.2 ppm. Here, we assumed that σ(II) was 0.4 ppm, which corresponds to 2σ.

For domain III (troposphere without observations above the PBL), the data sets containing observed data from the top of the PBL to the tropopause were chosen to evaluate the "true" partial XCO$_2$ of the whole troposphere above the PBL and the CO$_2$ concentrations at 5 km were compared with the partial XCO$_2$ calculated from the observed profile. Here, the CO$_2$ concentration at 5 km was assumed to be the partial XCO$_2$ when only one observation was available in the troposphere above the PBL. This analysis can determine the upper limit of uncertainties in domain III because nearly all data sets include many observations in the troposphere above the PBL. The comparison showed that the uncertainty in domain III was at most 1.5 ppm, so the assumption of 1.73 ppm (the standard deviation corresponding to a uniform distribution within ±3 ppm) is a good approximation, though slightly high.

For domain IV (stratosphere without observation data), it is difficult to obtain an "observed" partial XCO$_2$, so the difference between the uppermost observed data in the stratosphere and the nearest corrected age of air estimate from the ACTM was used. The standard deviations of the errors were from 1.5 to 2.0 ppm, so the assumption of 1.73 ppm appears reasonable.

The total uncertainties calculated (Eq. 2) from all of the profile assumptions were at most 2 ppm and typically between 0.5 and 1.0 ppm. The uncertainty values strongly depended on whether observations from the PBL were available. They were large at CONTRAIL sites where the lowermost observation altitudes were relatively high, often above the top of the PBL. At NRT, the use of Tsukuba tower data reduced the uncertainty to less than 1 ppm. When tower data were not available, the uncertainty at NRT was large. The uncertainties at NOAA and NIES sites were basically uniform with values less than 1 ppm. At the NOAA sites with the largest uncertainties (AAO, LEF,

SGP, and WGC), the uncertainties were nearly 1 ppm. At these sites, the uppermost observation altitude was typically ∼ 4000 m, which is lower than at the other sites and caused the uncertainties to be larger. At PFA, the uncertainties were also large, in this case because the height of the lowermost observation was often above the top of the

5 PBL. It is difficult to detect any seasonal behavior of the uncertainties at CONTRAIL sites, where the uppermost observation altitude was relatively high. For reference, frequency distributions of the estimated uncertainties at NRT, NGO, AAO, BNE, and SUR are shown in Fig. 5.

Araki et al. (2010) estimated the uncertainties derived from the CIRA-86 dry air num-

10 ber density data and the NCEP tropopause height data by comparing their results obtained with NCEP and CIRA-86 data with those obtained by using rawinsonde measurement data instead. They estimated the uncertainty from the CIRA-86 data to be 0.08 ppm, which is relatively insignificant compared with our estimated total uncertainties. They did not report the uncertainties from the NCEP tropopause heights, but they

15 estimated the uncertainties from both the NCEP tropopause height and their assumptions about profiles near the surface to be 0.92 ppm (Araki et al., 2010). Therefore, the uncertainties from the NCEP tropopause height were also small because the uncertainties from the profiles near the surface were dominant and can be treated as part of the uncertainties derived from the profile assumptions, as described above.

20 **5   Conclusions**

XCO$_2$ at 53 sites in the world was calculated from aircraft measurement data obtained by CONTRAIL, NOAA, and NIES between 2007 and 2009 along with tower data obtained at the surface and the ACTM simulated age of air to estimate profiles in the stratosphere. The amplitudes of seasonal cycles decreased from north to south. The

25 estimated upper limits of the uncertainties of XCO$_2$ were typically less than 1 ppm, suggesting that this data set is suitable for evaluation of XCO$_2$ estimates by satellites.

Recently, XCO_2 has been derived from data obtained by satellites, such as GOSAT (Yokota et al., 2009), the Scanning Imaging Absorption Spectrometer for Atmospheric Chartography (SCIAMACHY; Bovensmann et al., 1999) onboard ENVISAT, and the Atmospheric Infrared Sounder (AIRS; Crevosier et al., 2004) onboard NASA's Aqua platform. These satellite data are considered useful for decreasing the flux estimation errors in global atmospheric transport models and for investigating CO_2 sources and the carbon cycle in more detail. However, it is necessary to validate these data for such scientific applications. The profile data of aircraft measurements cannot be directly compared with the column-averaged data from satellites. In this work, we therefore propose a method for converting the profile data from aircraft to column-averaged data and for estimating the uncertainties of the calculated values. Our analysis suggests that the uncertainties are small enough for the aircraft data to be used for primary validation of satellite data. Furthermore, it should be possible to extend the method to other species such as methane using tracer-tracer correlation method.

References

Andrews, A. E., Boering, K. A., Daube, B. C., Wofsy, S. C., Loewenstein, M., Jost, H., Podolske, J. R., Webster, C. R., Herman, R. L., Scott, D. C., Flesch, G. J., Moyer, E. J., Elkins, J. W., Dutton, G. S., Hurst, D . F., Moore, F. L., Ray, E. A., Romashkin, P. A., and

Strahan, S. E.: Mean ages of stratospheric air derived from in situ observations of CO_2, CH_4, and N_2O, J. Geophys. Res., 106, 32295–32314, doi:10.1029/2001JD000465, 2001.

Andrews, A. E., Kofler, J., Bakwin, P. S., Zhao, C., and Tans, P.: Carbon dioxide and carbon monoxide dry air mole fractions from the NOAA ESRL tall tower network, 1992–2009, Version: 2011-08-31, available at: ftp://ftp.cmdl.noaa.gov/ccg/towers/, 2011.

Araki, M., Morino, I., Machida, T., Sawa, Y., Matsueda, H., Ohyama, H., Yokota, T., and Uchino, O.: CO_2 column-averaged volume mixing ratio derived over Tsukuba from measurements by commercial airlines, Atmos. Chem. Phys., 10, 7659–7667, doi:10.5194/acp-10-7659-2010, 2010.

Austin, J. and Li, F.: On the relationship between the strength of the Brewer-Dobson circulation and the age of stratospheric air, Geophys. Res. Lett., 33, L17807, doi:10.1029/2006GL026867, 2006.

Bovensmann, H., Burrows, J. P., Buchwitz, M., Frerick, J., Noël, S., Rozanov, V. V., Chance, K. V., Goede, A. P. H.: SCIAMACHY: mission objectives and measurement modes, J. Atmos. Sci., 56, 127–150, 1999.

COSPAR (Committee on Space Research): The COSPAR International Reference Atmosphere (CIRA-86), British Atmospheric Data Center, available at: http://badc.nerc.ac.uk/view/badc.nerc.ac.uk__ATOM__dataent_CIRA, 2012.

Crevoisier, C., Heilliette, S., Chédin, A., Serrar, S., Armante, R., and Scott, N. A.: Midtropospheric CO_2 concentration retrieval from AIRS observations in the tropics, Geophys. Res. Lett., 31, L17106, doi:10.1029/2004GL020141, 2004.

Engel, A., Möbius, T., Bönisch, H., Schmidt, U., Heinz, R., Levin, I., Atlas, E., Aoki, S., Nakazawa, T., Sugawara, S., Moore, F., Hurst, D., Elkins, J., Schauffler, S., Andrews, A., Boering, K.: Age of stratospheric air unchanged within uncertainties over the past 30 years, Nature Geoscience, 2, 28–31, doi:10.1038/ngeo388, 2009.

Fleming, E. L., Chandra, S., Shoeberl, M. R., and Barnett, J. J., Monthly mean global climatology of temperature, wind, geopotential height and pressure for 0–120 km, National Aeronautics and Space Administration, Technical Memorandum 100697, Washington, D. C., 1988.

Fleming, E. L., Chandra, S., Barnett, J. J., and Corney, M.: Zonal mean temperature, pressure, zonal wind and geopotential height as functions of latitude, Adv. Space Res., 10, 11–59, doi:10.1016/0273-1177(90)90386-E, 1990.

GMD Data Archive: Global Monitoring Division, Earth System Research Laboratory, NOAA, available: http://www.esrl.noaa.gov/gmd/dv/ftpdata.html, 2012.

Atmospheric XCO$_2$ from aircraft measurements

Y. Miyamoto et al.

Title Page

Abstract	Introduction
Conclusions	References
Tables	Figures

|◀ | ▶|

◀ | ▶

Back | Close

Full Screen / Esc

Printer-friendly Version

Interactive Discussion

Harnisch, J., Borchers, R., Fabian, P., and Maiss, M.: Tropospheric trends for CF_4 and C_2F_6 since 1982 derived from SF_6 dated stratospheric air, Geophys. Res. Lett., 23, 1099–1102, doi:10.1029/96GL01198, 1996.

Inoue, H. Y. and Matsueda, H.: Variations in atmospheric CO_2 at the Meteorological Research Institute, Tsukuba, Japan, J. Atoms. Chem., 23, 137–161, 1996.

Ishidoya, S., Sugawara, S., Morimoto, S., Aoki S., and Nakazawa T.: Gravitational separation of major atmospheric components of nitrogen and oxygen in the stratosphere, Geophys. Res. Lett., 35, L03811, doi:10.1029/2007GL030456, 2008.

Kalnay, E., Kanamitsu, M., and Baker, W. E.: Global numerical weather prediction at the National Meteorological Center, B. Amer. Meteor. Soc., 71, 1410–1428, 1990.

Kuze, A., Suto, H., Nakajima, M., and Hamazaki, T.: Thermal and near infrared sensor for carbon observation Fourier-transform spectrometer on the Greenhouse Gases Observing Satellite for greenhouse gases monitoring, Appl. Opt., 48, 6716–6733, doi:10.1364/AO.48.006716, 2009.

Machida, T., Nakazawa, T., Ishidoya, S., Maksyutov, S., Tohjima, Y., Takahashi, Y., Watai, T., Vinnichenko, N., Panchenko, M., Arshinov, M., Fedoseev, N., and Inoue, G.: Temporal and spatial variations of atmospheric CO_2 mixing ratio over Siberia, Proceedings of The Sixth International CO_2 Conference, 1–5 October, Sendai, Japan, 2001.

Machida, T., Matsueda, H., Sawa, Y., Nakagawa, Y., Hirotani, K., Kondo, N., Goto, K., Nakazawa, T., Ishikawa, K., and Ogawa, T.: Worldwide measurements of atmospheric CO_2 and other trace gas species using commercial airlines, J. Atmos. Oceanic. Technol., 25, 1744–1754, doi:10.1175/2008JTECHA1082.1, 2008.

Machida, T., Tohjima, Y., Katsumata, K., and Mukai, H.: A new CO_2 calibration scale based on gravimetric one-step dilution cylinders in National Institute for Environmental Studies – NIES 09 CO_2 scale, GAW Report, 194, 114–119, 15th WMO/IAEA Meeting of Experts on Carbon Dioxide, Other Greenhouse Gases and Related Tracers Measurement Techniques, WMO/TD No. 1553, 2011.

Miller, C. E., Crisp, D., DeCola, P. L., Olsen, S. C., Randerson, J. T., Michalak, A. M., Alkhaled, A., Rayner, P., Jacob, D. J., Suntharalingam, P., Jones, D. B. A., Denning, A. S., Nicholls, M. E., Doney, S. C., Pawson, S., Bösch, H., Connor, B. J., Fung, I. Y., O'Brien, D., Salawitch, R. J., Sander, S. P., Sen, B., Tans, P., Toon, G. C., Wennberg, P. O., Wofsy, S. C., Yung, Y. L., and Law, R. M.: Precision requirements for space-based XCO_2 data, J. Geophys. Res., 112, D10314, doi:10.1029/2006JD007659, 2007.

Atmospheric XCO2 from aircraft measurements

Y. Miyamoto et al.

Title Page

Abstract | Introduction

Conclusions | References

Tables | Figures

|◀ | ▶|

◀ | ▶

Back | Close

Full Screen / Esc

Printer-friendly Version

Interactive Discussion

Morino, I., Uchino, O., Inoue, M., Yoshida, Y., Yokota, T., Wennberg, P. O., Toon, G. C., Wunch, D., Roehl, C. M., Notholt, J., Warneke, T., Messerschmidt, J., Griffith, D. W. T., Deutscher, N. M., Sherlock, V., Connor, B., Robinson, J., Sussmann, R., and Rettinger, M.: Preliminary validation of column-averaged volume mixing ratios of carbon dioxide and methane retrieved from GOSAT short-wavelength infrared spectra, Atmos. Meas. Tech., 4, 1–16, doi:10.5194/amt-4-1-2011, 2011.

Nakazawa, T., Machida, T., Sugawara, S., Murayama, S., Morimoto, S., Hashida, G., Honda, H., and Itoh, T.: Measurements of the stratospheric carbon dioxide concentration over Japan using a balloon-borne cryogenic sampler, Geophys. Res. Lett., 22, 1229–1232, doi:10.1029/95GL01188, 1995.

NCEP: NOAA/National Weather Service, National Center for Environmental Prediction, NCEP Internet Services Team, available at: http://www.ncep.noaa.gov/, 2012.

NOAA/ESRL Carbon Cycle Greenhouse Gases Aircraft Program, available at: http://www.esrl.noaa.gov/gmd/ccgg/aircraft/index.html, 2012.

Patra, P. K., Lal, S., Subbaraya, B. H., Jackman, C. H., and Rajaratnam, P.: Observed vertical profile of sulphur hexafluoride (SF_6) and its atmospheric applications, J. Geophys. Res., 102, 8855–8859, 1997.

Patra, P. K., Maksyutov, S., Sasano, Y., Nakajima, H., Inoue, G., and Nakazawa, T.: An evaluation of CO_2 observations with solar occultation FTS for inclined-orbit satellite sensor for surface source inversion, J. Geophys. Res., 108, D24, 4759, doi:10.1029/2003JD003661, 2003.

Patra, P. K., Takigawa, M., Dutton, G. S., Uhse, K., Ishijima, K., Lintner, B. R., Miyazaki, K., and Elkins, J. W.: Transport mechanisms for synoptic, seasonal and interannual SF_6 variations and "age" of air in troposphere, Atmos. Chem. Phys., 9, 1209–1225, doi:10.5194/acp-9-1209-2009, 2009.

Rayner, P. J., Law, R. M., O'Brien, D. M., Butler, T. M., and Dilley, A. C.: Global observations of the carbon budget 3. Initial assessment of the impact of satellite orbit, scan geometry, and cloud on measuring CO_2 from space, J. Geophys. Res., 107, D21, doi:10.1029/2001JD000618, 2002.

Schneising, O., Bergamaschi, P., Bovensmann, H., Buchwitz, M., Burrows, J. P., Deutscher, N. M., Griffith, D. W. T., Heymann, J., Macatangay, R., Messerschmidt, J., Notholt, J., Rettinger, M., Reuter, M., Sussmann, R., Velazco, V. A., Warneke, T., Wennberg, P. O., and Wunch, D.: Atmospheric greenhouse gases retrieved from

Atmospheric XCO$_2$ from aircraft measurements

Y. Miyamoto et al.

Title Page

Abstract | Introduction

Conclusions | References

Tables | Figures

◄ | ►

◄ | ►

Back | Close

Full Screen / Esc

Printer-friendly Version

Interactive Discussion

SCIAMACHY: comparison to ground-based FTS measurements and model results, Atmos. Chem. Phys., 12, 1527–1540, doi:10.5194/acp-12-1527-2012, 2012.

Sela, J.: Spectral modeling at the National Meteorological Center, Mon. Weather Rev., 108, 1279–1292, 1980.

5 Tans, P. P., Bakwin, P. S., Conway, T. J., Dissly, R. W., Dlugokencky, E. J., Geller, L. S., Guenther, D. W., Hurst, D. F., Kitzis, D. R.., Lang, P. M., Masarie, K. A., Miller, J. B., Novelli, P. C., Prostko-Bell, C., Ramonet, M., Thoning, K. W., Trolier, M., Waterman, L. S., Zhang, N., and Zhao, C.: Carbon Cycle (Group Report), Climate Monitoring and Diagnostics Laboratory, No. 23, Summary Report 1994–1995, edited by: Hoffman, D. J., Peterson, J. T., and

10 Rosson, R. M., US Department of Commerce, Boulder, CO, 1996.

WDCGG: WMO Global Atmosphere Watch, World Data Centre for Greenhouse Gases, available at: http://ds.data.jma.go.jp/gmd/wdcgg/, 2012.

WMO: WMO Greenhouse Gas Bulletin, No. 3, World Meteorological Organization, 2006, available at: http://www.wmo.int/pages/prog/arep/gaw/ghg/GHGbulletin.html, 2012.

15 Wunch, D., Toon, G. C., Wennberg, P. O., Wofsy, S. C., Stephens, B. B., Fischer, M. L., Uchino, O., Abshire, J. B., Bernath, P., Biraud, S. C., Blavier, J.-F. L., Boone, C., Bowman, K. P., Browell, E. V., Campos, T., Connor, B. J., Daube, B. C., Deutscher, N. M., Diao, M., Elkins, J. W., Gerbig, C., Gottlieb, E., Griffith, D. W. T., Hurst, D. F., Jiménez, R., Keppel-Aleks, G., Kort, E. A., Macatangay, R., Machida, T., Matsueda, H., Moore, F., Morino, I., Park, S.,

20 Robinson, J., Roehl, C. M., Sawa, Y., Sherlock, V., Sweeney, C., Tanaka, T., and Zondlo, M. A.: Calibration of the Total Carbon Column Observing Network using aircraft profile data, Atmos. Meas. Tech., 3, 1351–1362, doi:10.5194/amt-3-1351-2010, 2010.

Wunch, D., Toon, G. C., Blavier, J.-F. L., Washenfelder, R. A., Notholt, J., Connor, B. J., Griffith, D. W. T., Sherlock, V., and Wennberg, P. O.: The Total Carbon Column Observing Net-

25 work, Philos. T. Roy. Soc. A, 369, 2087–2112, doi:10.1098/rsta.2010.0240, 2011a.

Wunch, D., Wennberg, P. O., Toon, G. C., Connor, B. J., Fisher, B., Osterman, G. B., Frankenberg, C., Mandrake, L., O'Dell, C., Ahonen, P., Biraud, S. C., Castano, R., Cressie, N., Crisp, D., Deutscher, N. M., Eldering, A., Fischer, M. L., Griffith, D. W. T., Gunson, M., Heikkinen, P., Keppel-Aleks, G., Kyrö, E., Lindenmaier, R., Macatangay, R., Mendonca, J., Messer-

30 schmidt, J., Miller, C. E., Morino, I., Notholt, J., Oyafuso, F. A., Rettinger, M., Robinson, J., Roehl, C. M., Salawitch, R. J., Sherlock, V., Strong, K., Sussmann, R., Tanaka, T., Thompson, D. R., Uchino, O., Warneke, T., and Wofsy, S. C.: A method for evaluating bias in global

measurements of CO_2 total columns from space, Atmos. Chem. Phys., 11, 12317–12337, doi:10.5194/acp-11-12317-2011, 2011b.

Yang, F., Pan, H.-L., Krueger, S. K., Moorthi, S., and Lord, S. J.: Evaluation of the NCEP global forecast system at the ARM SGP site, Mon. Weather Rev., 134, 3668–3690, 2006.

Yokota, T., Yoshida, Y., Eguchi, N., Ota, Y., Tanaka, T., Watanabe, H., and Maksyutov, S.: Global concentrations of CO_2 and CH_4 retrieved from GOSAT: first preliminary results, SOLA, 5, 160–163, doi:10.2151/sola.2009-041, 2009.

Yoshida, Y., Ota, Y., Eguchi, N., Kikuchi, N., Nobuta, K., Tran, H., Morino, I., and Yokota, T.: Retrieval algorithm for CO_2 and CH_4 column abundances from short-wavelength infrared spectral observations by the Greenhouse gases observing satellite, Atmos. Meas. Tech., 4, 717–734, doi:10.5194/amt-4-717-2011, 2011.

Zhu, X., Yee, J.-H., and Strobel, D. F.: Middle atmosphere age of air in a globally balanced two-dimensional model, J. Geophys. Res., 105, 15201–15212, 2000.

Title Page

Abstract | Introduction

Conclusions | References

Tables | Figures

◀ | ▶

◀ | ▶

Back | Close

Full Screen / Esc

Printer-friendly Version

Interactive Discussion

Table 1. Locations of the sites where aircraft measurements were made.

(a) CONTRAIL CODE	Latitude (° N)	Longitude (° E)	
AMS	52.3	4.8	Schiphol Airport, the Netherlands
LHR	51.5	−0.5	Heathrow Airport, UK
YVR	49.2	−123.2	Vancouver International Airport, Canada
CDG	49.0	2.5	Charles de Gaulle International Airport, France
MXP	45.6	8.7	Milan Malpensa International Airport, Italy
CTS	42.8	141.7	New Chitose Airport, Japan
FCO	41.8	12.3	Fiumicino Airport, Italy
ICN	37.5	126.5	Incheon International Airport, South Korea
NRT	35.8	140.4	Narita International Airport, Japan
HND	35.6	139.8	Tokyo International Airport, Japan
NGO	34.9	136.8	Chubu Centrair International Airport, Japan
ITM	34.8	135.4	Osaka International Airport, Japan
HIJ	34.4	132.9	Hiroshima Airport, Japan
KIX	34.4	135.2	Kansai International Airport, Japan
FUK	33.6	130.5	Fukuoka Airport, Japan
DEL	28.6	77.1	Indira Gandhi International Airport, India
OKA	26.2	127.6	Naha Airport, Japan
TPE	25.1	121.2	Taiwan Taoyuan International Airport, Taiwan
HNL	21.3	−157.9	Honolulu International Airport, USA
MEX	19.4	−99.1	Mexico City International Airport, Mexico
MNL	14.5	121.0	Ninoy Aquino International Airport, Philippines
BKK	13.7	100.7	Suvarnabhumi International Airport, Thailand
GUM	13.5	144.8	Guam International Airport, USA
SIN	1.4	104.0	Singapore Changi International Airport, Singapore
CGK	−6.1	106.7	Jakarta International Soekarno-Hatta Airport, Indonesia
DPS	−8.7	115.2	Ngurah Rai Airport, Indonesia
BNE	−27.4	153.1	Brisbane Airport, Australia
SYD	−33.9	151.2	Kingsford Smith Airport, Australia

Table 1. (Continued.)

(b) NOAA CODE	Latitude (°N)	Longitude (°E)	
AAO	40.1	−88.6	Airborne Aerosol Observing, Illinois
BNE	40.8	−97.2	Beaver Crossing, Nebraska
BRM	54.3	−105.0	Berms, Saskatchewan
CAR	40.4	−104.3	Briggsdale, Colorado
CMA	38.8	−74.3	Cape May, New Jersey
DND	48.4	−97.8	Dahlen, North Dakota
ESP	49.6	−126.4	Estevan Point, British Columbia
HAA	21.2	−159.0	Molokai Island, Hawaii
HFM	42.5	−72.2	Harvard Forest, Massachusetts
HIL	40.1	−87.9	Homer, Illinois
LEF	45.9	−90.3	Park Falls, Wisconsin
NHA	43.0	−70.6	Worcester, Massachusetts
PFA	65.1	−147.3	Poker Flat, Alaska
RTA	−21.3	−159.8	Rarotonga, Cook Islands
SCA	32.8	−79.6	Charleston, South Carolina
SGP	36.8	−97.5	Southern Great Plains, Oklahoma
TGC	27.7	−96.9	Sinton, Texas
THD	41.1	−124.2	Trinidad Head, California
VAA	32.9	−79.4	Cartersville, Georgia
WBI	41.7	−91.4	West Branch, Iowa
WGC	38.3	−121.5	Walnut Grove, California

(c) NIES CODE	Latitude (°N)	Longitude (°E)	
SGM	35.1	139.3	Sagami Bay, Japan
YAK	62	130	Yakutsk, Russia
NOV	55	83	Novosibirsk, Russia
SUR	61	73	Surgut, Russia

Title Page

Abstract | Introduction

Conclusions | References

Tables | Figures

|◄ | ►|

◄ | ►

Back | Close

Full Screen / Esc

Printer-friendly Version

Interactive Discussion

Table 2. The assumed standard deviations of partial XCO$_2$ in each domain.

Domain	Standard deviation (ppm)
I (No observed data in PBL)	15
I (With observed data in PBL)	2.89
II	0.4
III	1.73
IV	1.73
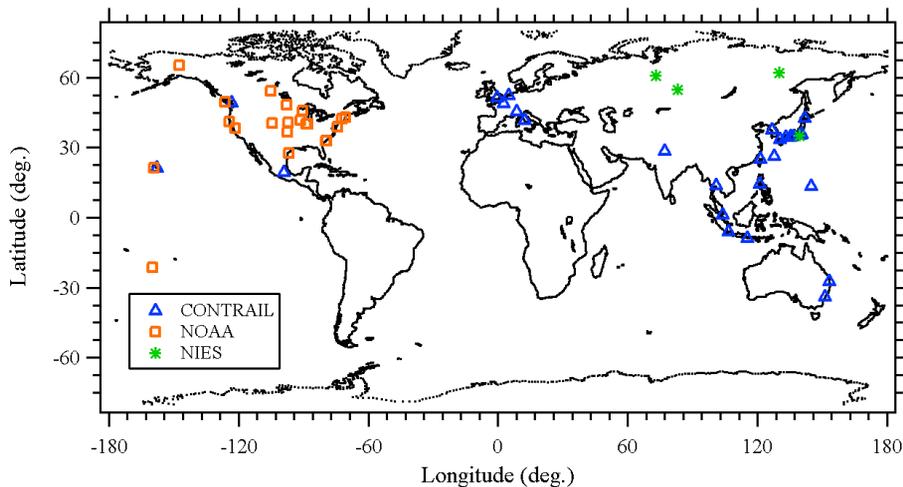
Fig. 1. Observation sites used in this study. Open triangles, open squares, and asterisks indicate CONTRAIL, NOAA, and NIES sites, respectively.
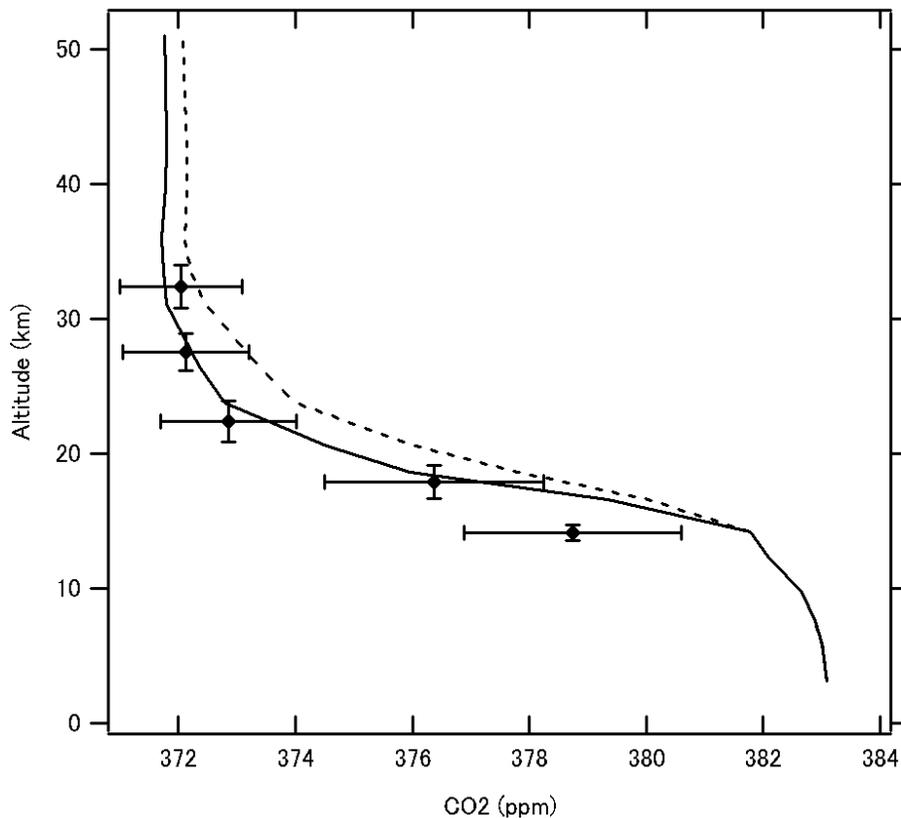
Fig. 2. Calculated CO_2 profile at 40.5° N latitude from the modeled "age of air" (lines) and the observed profile (symbols) at Sanriku, Japan (39.2° N) in January 2007. The dashed line shows the ACTM modeled profile uncorrected by the observed SF_6 age of air, and the solid line shows the profile after normalization. Error bars of the observed data show the standard deviations of the mean.

Discussion Paper | Discussion Paper | Discussion Paper | Discussion Paper |

ACPD

12, 28493–28523, 2012

Atmospheric XCO₂ from aircraft measurements

Y. Miyamoto et al.

Title Page

Abstract | Introduction

Conclusions | References

Tables | Figures

◄ | ►

◄ | ►

Back | Close

Full Screen / Esc

Printer-friendly Version

Interactive Discussion

Full Screen / Esc

Printer-friendly Version

Interactive Discussion
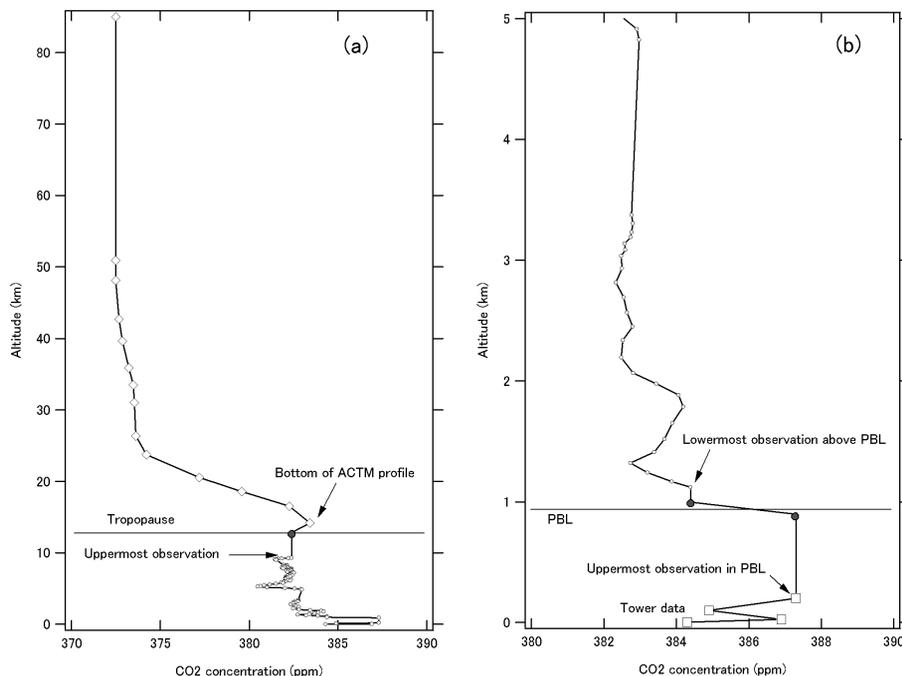
Fig. 3. Schematic example of a vertical CO_2 profile: **(a)** the profile from the ground to 85 km; **(b)** an expanded view of the profile between the ground and 5 km. Open circles, squares, and diamonds show data observed by aircraft, data observed by towers, and the ACTM profile, respectively. Closed circles show the assumed value at the tropopause and the top of the PBL.
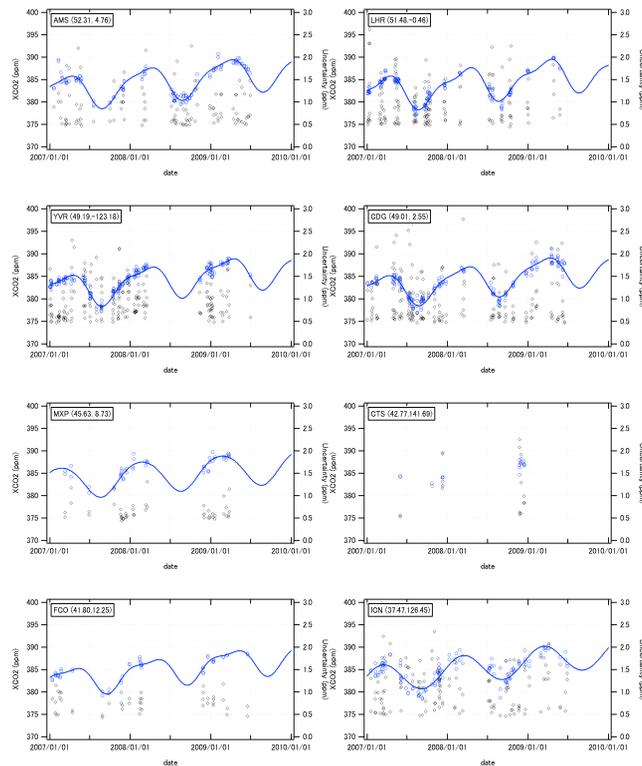
Fig. 4. Calculated XCO$_2$ values and their estimated uncertainties at each site. The site code (Table 1) and its latitude and longitude are shown at the upper left corner of each panel. Blue circles show XCO$_2$ (left axis), and black rhomboids show their uncertainties (right axis). Blue solid lines show curves fitted to the temporal behavior of XCO$_2$ as a visual guide (only for sites where the number of data was sufficient).

Fig. 4. (Continued.)

Atmospheric XCO₂ from aircraft measurements

Y. Miyamoto et al.

Title Page

Abstract | Introduction

Conclusions | References

Tables | Figures

◄ | ►

Back | Close

Full Screen / Esc

Printer-friendly Version

Interactive Discussion

Fig. 4. (Continued.)

Fig. 4. (Continued.)

[◄◄](#)   [►►](#)

[◄](#)   [►](#)

[Back](#)   [Close](#)

[Full Screen / Esc](#)

[Printer-friendly Version](#)

[Interactive Discussion](#)
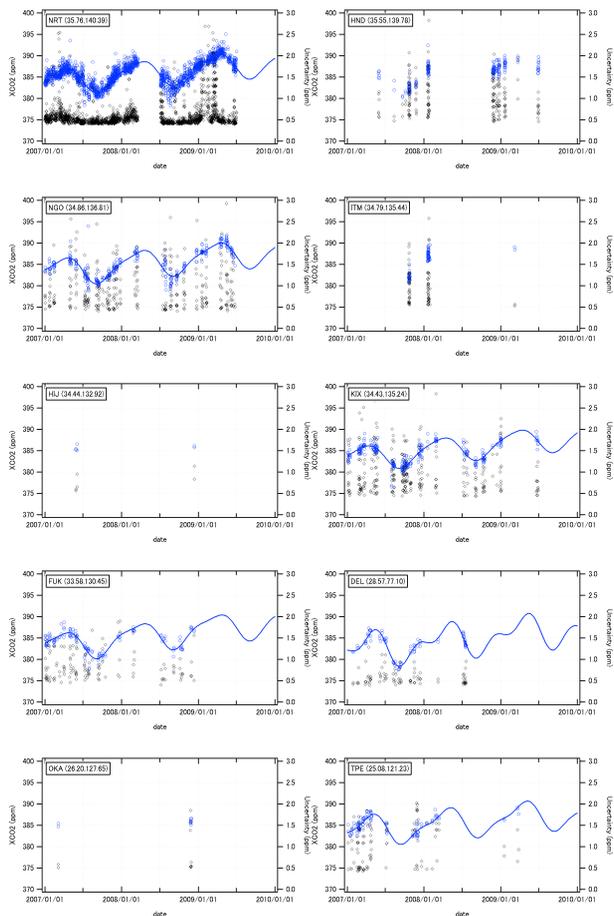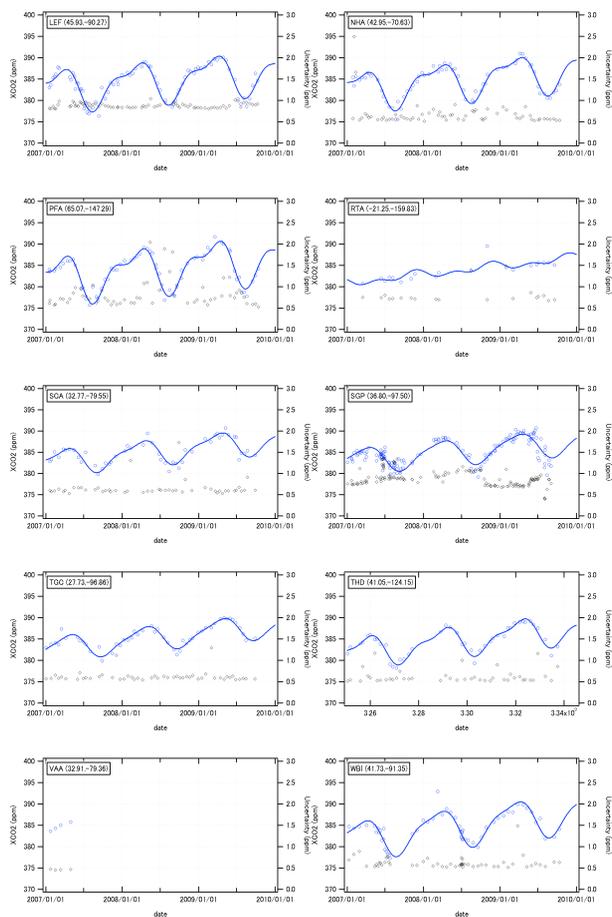
Fig. 4. (Continued.)

Title Page

Abstract | Introduction

Conclusions | References

Tables | Figures

|◄ | ►|

◄ | ►

Back | Close

Full Screen / Esc

Printer-friendly Version

Interactive Discussion

Fig. 4. (Continued.)

Full Screen / Esc

Printer-friendly Version

Interactive Discussion

CONTRAIL

NRT (35.76,140.39)
average = 0.58
standard deviation = 0.26

NGO (34.86,136.81)
average = 0.95
standard deviation = 0.50

NOAA

BNE (40.80,−97.18)
average = 0.58
standard deviation = 0.12

SGP (36.80,−97.50)
average = 0.89
standard deviation = 0.19

NIES

SUR (61.00,73.00)
average = 0.69
standard deviation = 0.10
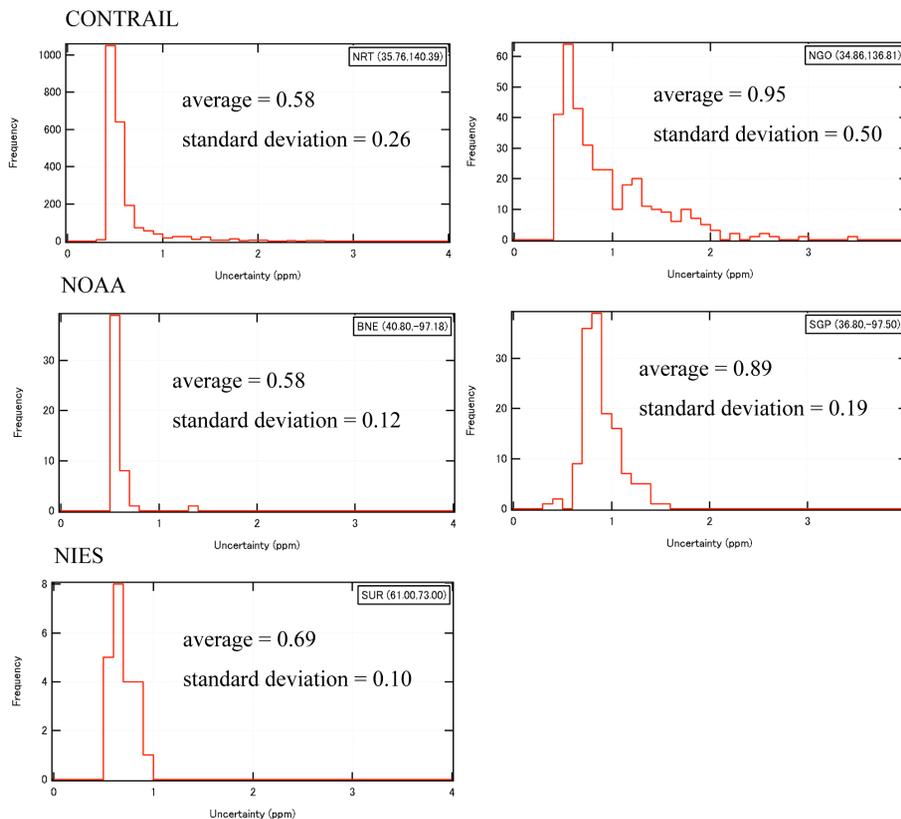
Fig. 5. Frequency distributions of the estimated uncertainties at five sites. The size of each frequency class is 0.2 ppm.